

# EIS measurement for corrosion monitoring under multiphase flow conditions

Y. Chen\*, W.P. Jepson

*NSF I/UCRC, Corrosion in Multiphase Systems Center, Department of Chemical Engineering, Ohio University, Athens, OH 45701, USA*

Received 7 August 1998; received in revised form 28 January 1999

---

## Abstract

The electrochemical behavior of carbon steel in ASTM saltwater saturated with carbon dioxide (CO<sub>2</sub>) with/without an imidazoline based inhibitor under different flow conditions was studied using Electrochemical Impedance Spectroscopy (EIS). The effects of the addition of a light refined oil on the inhibitor performance were examined. Experiments were carried out in a 101.6 mm I.D., 15 m long acrylic flow loop. The system was maintained at a pressure of 0.136 MPa and temperature of 40°C. Experiments were conducted at water cuts of 100 and 80%. Inhibitor concentrations of 25 ppm and 100 ppm were used. Results show that the EIS technique can be used to study mechanisms of corrosion and its inhibition in turbulent multiphase flow conditions. It was seen that the high rate of shear stress and turbulence in multiphase flows can significantly enhance the corrosion rate and reduce the inhibition performance of corrosion inhibitors. © 1999 Elsevier Science Ltd. All rights reserved.

**Keywords:** Electrochemical Impedance Spectroscopy (EIS); Carbon dioxide corrosion; Corrosion inhibitor; Multiphase flow; Large diameter flow loop

---

## 1. Introduction

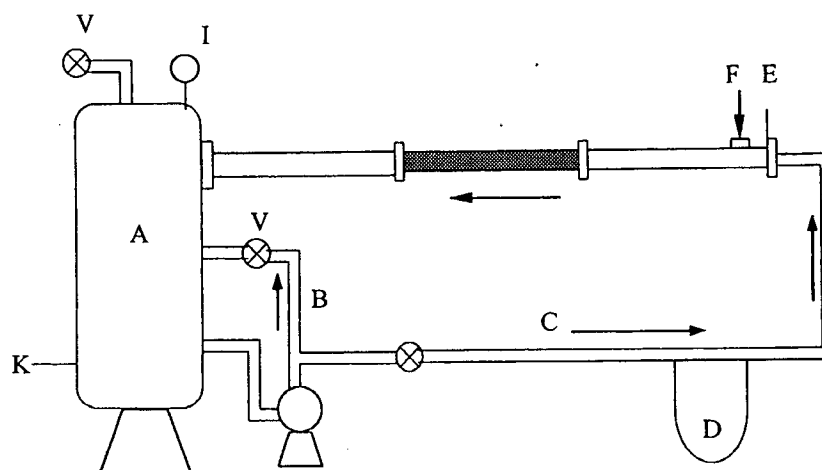
In remote and offshore oil sites, the product from the wells is transported as a mixture of oil, saltwater and natural gas. Carbon dioxide in the natural gas dissolves in saltwater and results in the formation of a weak carbonic acid often causing severe corrosion in carbon steel pipelines. This problem has caused the consideration of many corrosion control methods for oil fields. Chemical inhibitors have become important for corrosion control. The successful selection of inhibitors depends on a clear understanding of the operational conditions, such as operating temperature and

pressure, fluid properties, solution pH and chemistry and flow conditions. Flow conditions include flow velocity, single/multiphase flow, and composition of the multiphase mixture [1]. Inability to predict the effects of multiphase flow patterns on inhibitors in pipelines can seriously degrade the effectiveness of the inhibitor [2].

Multiphase flow is characterized by many different flow regimes. These depend on the flow rate of gas, oil and water for three-phase systems. At high oil production rates, the slug flow regime is prominent [3]. Slug flow is known to enhance internal corrosion in multiphase pipelines [4-6]. The high rate of shear and turbulence due to the mixing vortex and the bubble impact in the mixing zone of slug can increase the corrosion rate or reduce the performance of inhibitors

---

\* Corresponding author.



- |                                     |                   |
|-------------------------------------|-------------------|
| A. Liquid tank                      | G. Test section   |
| B. Bypass                           | H. Gas outlet     |
| C. Liquid feed                      | I. Pressure gauge |
| D. Orifice plate with mercury meter | K. Heater         |
| E. Flow height control gate         | V. Valves         |
| F. Gas input                        |                   |

Fig. 1. Experimental system.

that might have otherwise formed on the pipe wall [7]. The flow characteristics in slug flow are characterized by a dimensionless Froude number [3] and the turbulence levels and bubble impact on the pipe wall increase with increase in Froude number.

Corrosion inhibitor evaluations in  $\text{CO}_2$  corrosion conditions have been studied extensively by many researchers [8,9]. These studies were carried out in Rotating Cylinder Electrode (RCE) systems or in small-scale flow loops. These systems cannot completely simulate actual field conditions. They ultimately provide only a qualitative ranking of conditions and inhibitors. The studies on corrosion and inhibition in large diameter flow loops under multiphase flow conditions have become a critical step of corrosion control in practical oil field.

Electrochemical Impedance Spectroscopy (EIS) technique is very useful for evaluation of inhibitor performances, analysis of electrochemical mechanisms and corrosion processes. Equivalent circuit models provide a helpful way to interpret and quantify the EIS spectra if the physical models are understood. This paper demonstrates the ability of this technique to study corrosion and inhibition mechanisms in multiphase flow environments and proposes equivalent circuit models to analyze experimental data under different flow conditions with or without inhibitors.

## 2. Experimental setup

Experiments were carried out in a 101.6 mm I.D., 15 m long acrylic pipeline. The schematic layout of the system is shown in Fig. 1. A specific mixture of oil and saltwater is placed in the 1.4 m<sup>3</sup> stainless steel tank A. The liquid from the tank is pumped into the 76 mm I.D. PVC pipe by a 1.5 kW centrifugal pump. The flow rate of the liquid is controlled by a bypass line B and is measured by a calibrated orifice meter D. The liquid is forced under gate E into the 101.6 mm I.D. Plexiglas pipe where it formed a fast moving liquid film. The carbon-dioxide gas is also introduced into the system at port E. The gas-liquid mixture passes through the Plexiglas pipeline and enters the tank where the liquid is separated using a de-entrained plate inside the tank. Liquid is recycled and gas is vented to the atmosphere through the exhausted at the top of the tank. The carbon dioxide gas is also used to pressurize the system. The pressure inside the tank is indicated by the gauge I, installed on the top of the tank. All the measurements are taken in the test section G located 8 m downstream from the gate. For slug flow, a hydraulic jump [3] is generated and moved into the test section by controlling the gas flow at the inlet F. The liquid inside the tank is heated by two 1.5 kW heaters positioned at K.

The EIS probe and coupons were inserted into the

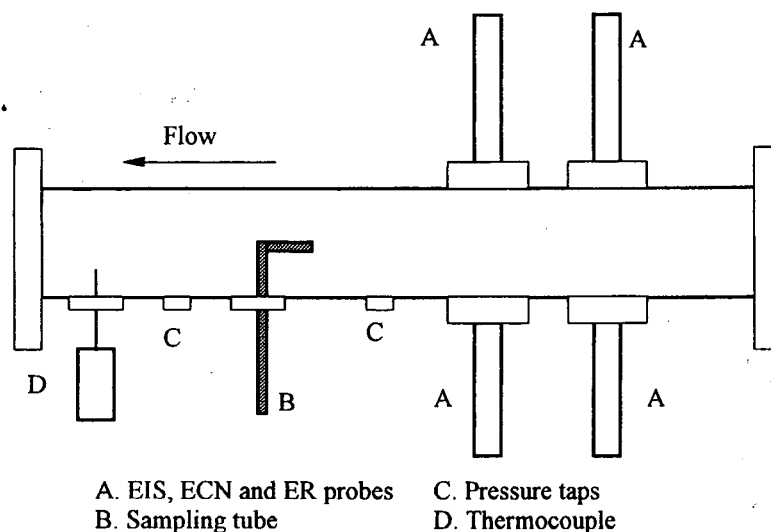
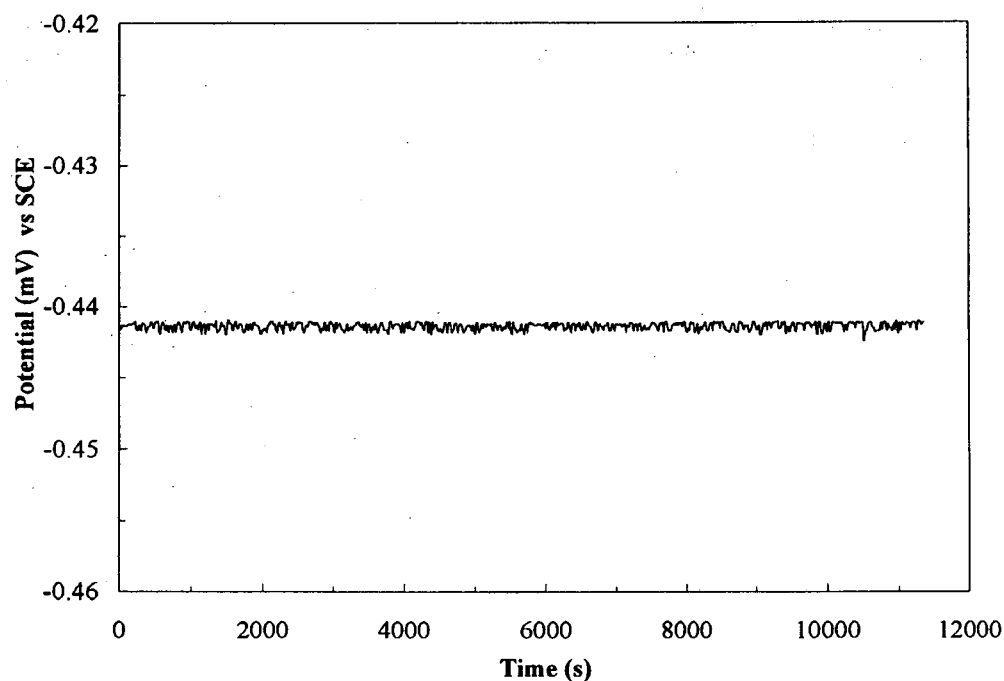


Fig. 2. Test section.

test section G shown in Fig. 2, are mounted flush with the pipe wall. The ac impedance spectra in this work were generated by GAMRY CMS300 corrosion monitoring system and analyzed using their accompanying software. EIS measurements were carried out at an open circle potential with 10 mV ac potential in the frequency range from 20 mHz to 5 kHz.

Preliminary studies were made in a Rotating

Cylinder Electrode (RCE) system. Fig. 3 shows the steady open circuit potential of stainless steel in 100% ASTM substitute saltwater saturated with  $\text{CO}_2$ . The test was carried out at the constant temperature of  $40^\circ\text{C}$  and at stirring speed of 1000 rpm. The counter electrodes (CE) are two graphite rods, the reference electrode (RE) is a Saturated Calomel electrode (SCE) and the working electrode (WE) is 316 L stainless steel

Fig. 3. Open circuit potential vs time for 316 L stainless steel exposed to  $\text{CO}_2$ -saturated ASTM saltwater in the RCE system.

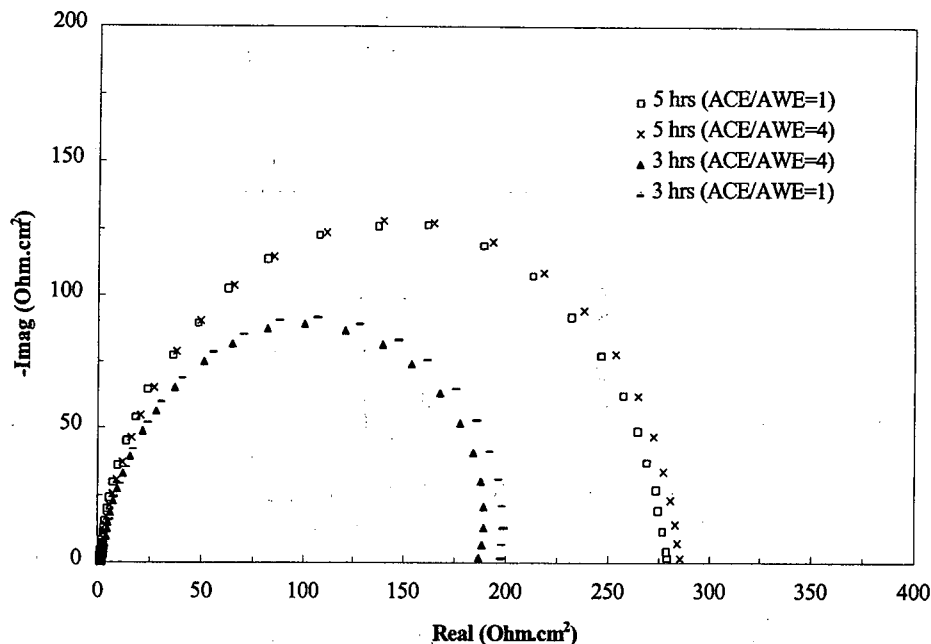


Fig. 4. Nyquist plots of EIS spectra for different area ratio of CE and WE in 100% ASTM saltwater RCE system.

with an area of  $3.02 \text{ cm}^2$ , which was polished with 600 grid sandpaper. This figure shows that 316 L is acceptable as reference electrode in ASTM saltwater. The Nyquist plots for a CE with 4 times as large an area as the WE and CE with the same area as WE is shown in Fig. 4 at exposure times of 3 and 5 h, respectively. The tests were conducted using C-1018 mild steel as WE with area of  $3.02 \text{ cm}^2$ , 316 L stainless steel as CE and SCE as RE. The Nyquist plots seem to be almost the

same for the different area ratio of CE to WE at both exposure times. This indicates the fact that the impedance of counter electrode is not influencing the test results. The EIS probe used in the multiphase flow loop consists of three electrodes as shown in Fig. 5. The working electrode is made of C-1018 carbon steel. The counter and reference electrodes are made of 316 L stainless steel. The surface area of each electrode is  $0.7854 \text{ cm}^2$  (diameter is 10 mm). The distance between centers of every two electrode is about 13 mm.

Studies were carried out using ASTM substitute saltwater, light hydrocarbon oil (Conoco LVT 200 with density of  $825 \text{ kg/m}^3$  and viscosity of 2 cp) and carbon dioxide gas. Once the de-oxygenation process was complete, the EIS probe, which was polished by 600-grid sandpaper, rinsed with acetone and distilled water for several times, was inserted into the test section and measurements were started. For the inhibition experiments, the inhibitor was injected into system and fully mixed with testing solution before the EIS probe installed. The experiments were made for water cuts of 100 and 80%. One imidazoline inhibitor formulated with imidazoline salt and quaternary amine was used at the concentration of 25 and 100 ppm. Full pipe flow was studied for liquid velocities of 0.5, 1.0 and 1.5 m/s and slug flow for Froude numbers of 4, 6 and 9. The system temperature and pressure are maintained constant at  $40^\circ\text{C}$  and 0.136 MPa for all experiments.

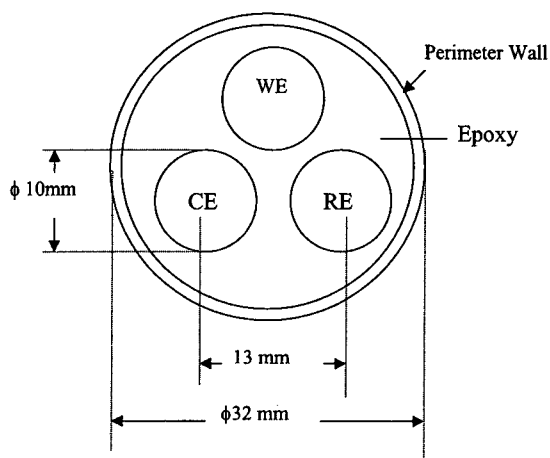


Fig. 5. EIS probe used in flow loop system.

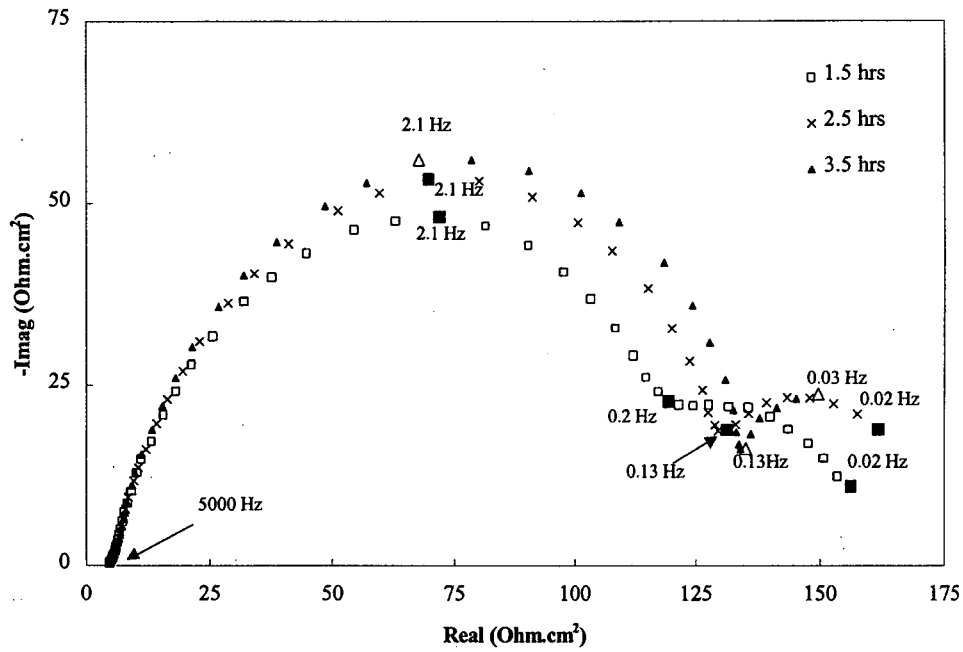


Fig. 6. Nyquist plots of EIS spectra for 1.5 m/s full pipe flow at different exposure times in 100% ASTM saltwater flow loop system.

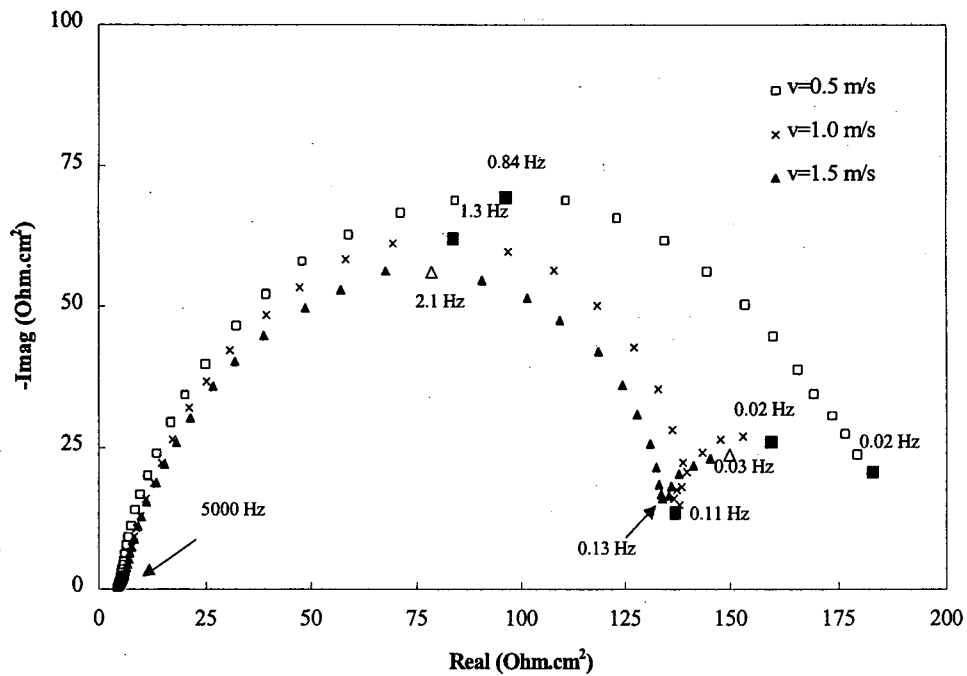


Fig. 7. Nyquist plots of EIS spectra for full pipe flow at different liquid velocities in 100% ASTM saltwater flow loop system.

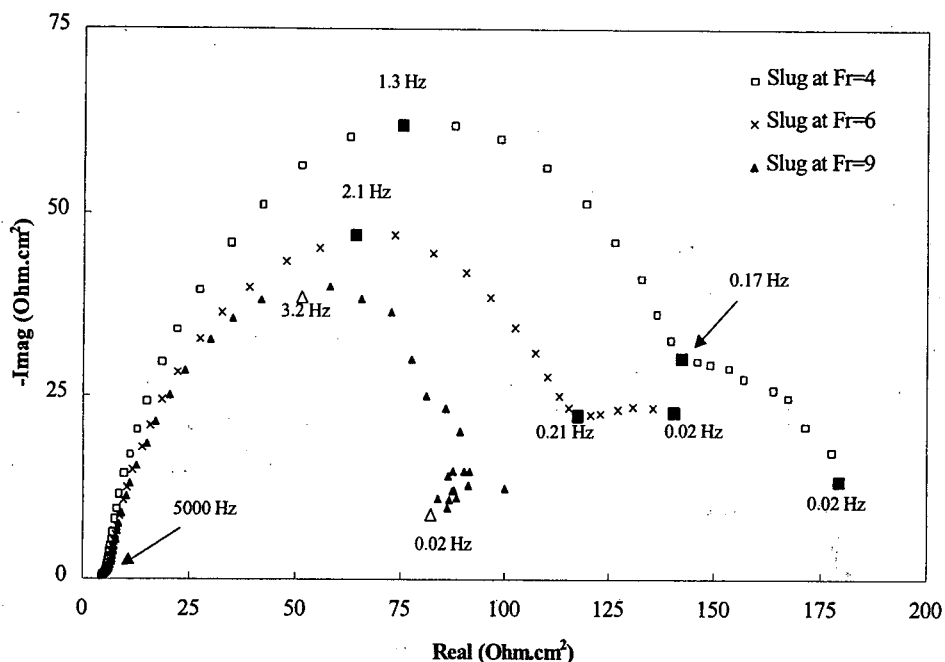


Fig. 8. Nyquist plots of EIS spectra for slug flow at different Froude numbers in 100% ASTM saltwater flow loop system.

### 3. Results and discussion

#### 3.1. 100% water-cut tests without inhibitor

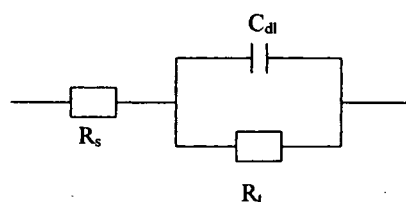
Initially, experiments were carried out in an RCE system and results similar to those in Fig. 4 were obtained. Here, single semicircular spectra are present, which indicate that the system can be described by a single time constant model. Later, single phase full pipe and slug flow were studied.

Fig. 6 shows Nyquist plots of EIS spectra under the full pipe flow at 1.5 m/s superficial liquid velocity for different exposure times. When compared to Fig. 4 for an RCE system, the impedance spectra do not exhibit single semicircles centered on the real axis. A second loop has begun to appear at low frequencies after an exposure time of 1.5 h. These might suggest that there is an additional electrochemical process other than the interfacial charge transfer reaction due to the presence of a porous corrosion product layers adjacent to the metal surface. These additional loops suggest that a second time constant is present. The distance along the real axis where the second loop appears increases with exposure time, which indicates the charge transfer resistance increases with time.

Fig. 7 shows the plots for full pipe flow at different superficial liquid velocities after exposure time of 3.5 h. It is seen that a depressed semicircular first loop is present for all liquid velocities and the formation of a second loop at low frequency region exists in full pipe

flow at liquid velocity of 1.0 and 1.5 m/s. For the lowest liquid velocity of 0.5 m/s, the second time constant at low frequency was unable to be detected at the low

(A)



(B)

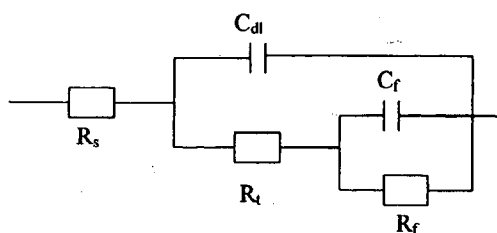


Fig. 9. Equivalent circuit models used for analyzing EIS data in 100% ASTM saltwater flow loop system.  $R_s$ , solution resistance;  $R_t$ , charge transfer resistance;  $C_{dl}$ , double layer capacitance;  $R_f$  and  $C_f$ , corrosion product film resistance and capacitance.

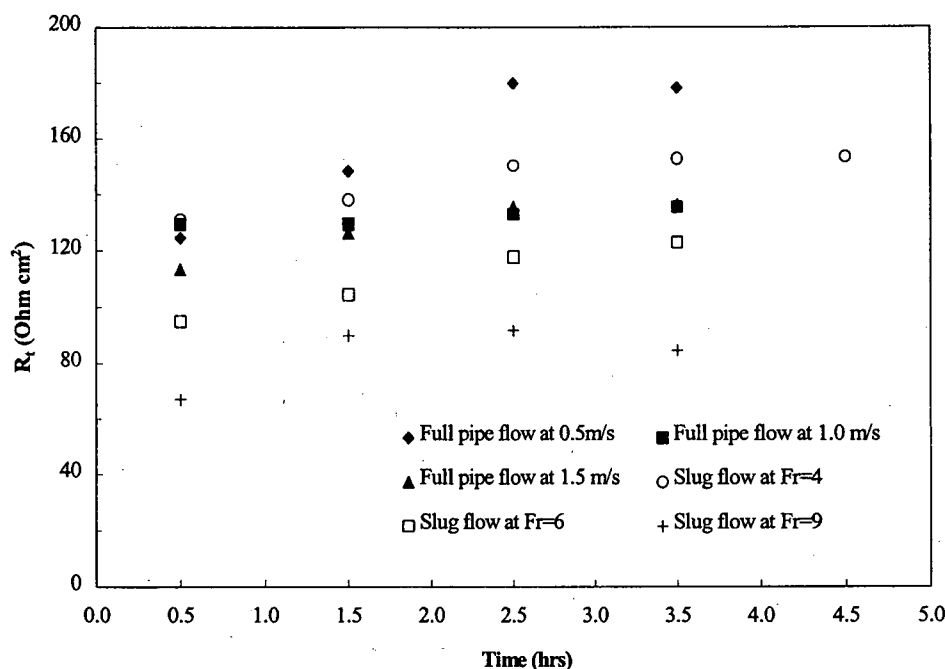


Fig. 10. Charge transfer resistance vs time for different flow conditions in 100% ASTM saltwater flow loop system.

frequency used in those tests. This could be due to a thin or undetectable corrosion product layer at this liquid velocity. The place on the real axis at which the second loop begins decreases to lower values with increase in liquid velocity.

It is well known that the mass transfer coefficient is higher at the higher liquid velocity [10]. For the case of full pipe flow at the higher liquid velocity, corrosive species could reach the metal surface faster. Hence, a lower charge transfer resistance is seen.

The EIS Nyquist plots for slug flow at different Froude numbers are shown in Fig. 8. Again, a depressed loop is found for these three flow conditions and the second loop is seen for slug flow at Froude numbers of 4 and 6. The data at the lower frequency for Froude number 9 shows more fluctuations which is due to the much higher rate of turbulence and bubble impact in the mixing zone of the slug. In highly turbulent slug flow, the shear stress at the bottom of the pipe is very high and the impact of the bubbles produces a cavitation-type effect [7]. These can remove the corrosion products and allow the corrosion to continue at a high rate. Therefore, only a thin or an undetectable corrosion product layer is present in slug flow at this Froude number. Compared to Froude numbers of 4 and 6, the charge transfer resistance for Froude number 9 slug flow is the lowest due to the highest rate of shear stress and turbulence. Flow conditions of

slug at Froude number 4 is similar to full pipe flow. The bubbles do not reach the bottom of the pipe due to the lower turbulence. The charge transfer resistance decreases with increase in Froude number.

The equivalent circuit models as shown in Fig. 9 are proposed to describe the corrosion process under multiphase flow conditions. Here  $R_s$  is the solution resistance,  $R_t$  is the charge transfer resistance and  $C_{dl}$  is the double layer capacitance that characterizes the charge separation between metal and electrolyte interface. However the double layer capacitor does not behave ideally due to the roughness caused by the corrosion product layer. The impedance of a capacitor has the form,

$$Z = A(j\omega)^{-\alpha}$$

For an ideal capacitor, the constant  $A$  is equal to  $1/C$  and  $\alpha = 1$ . For a non-ideal capacitor, the value of  $\alpha$  is less than one. The use of  $\alpha$  is only a description of non-ideal behavior of the double layer but its physical meaning is not clear [11]. With increasing corrosion product layer presence, another electrochemical process is seen, and is represented by the second  $R_f-C_f$  loop nested in the typical charge transfer  $R_t-C_{dl}$  network as shown in circuit.

Fig. 10 shows that charge transfer resistance,  $R_t$ , vs time under different flow conditions. This parameter is

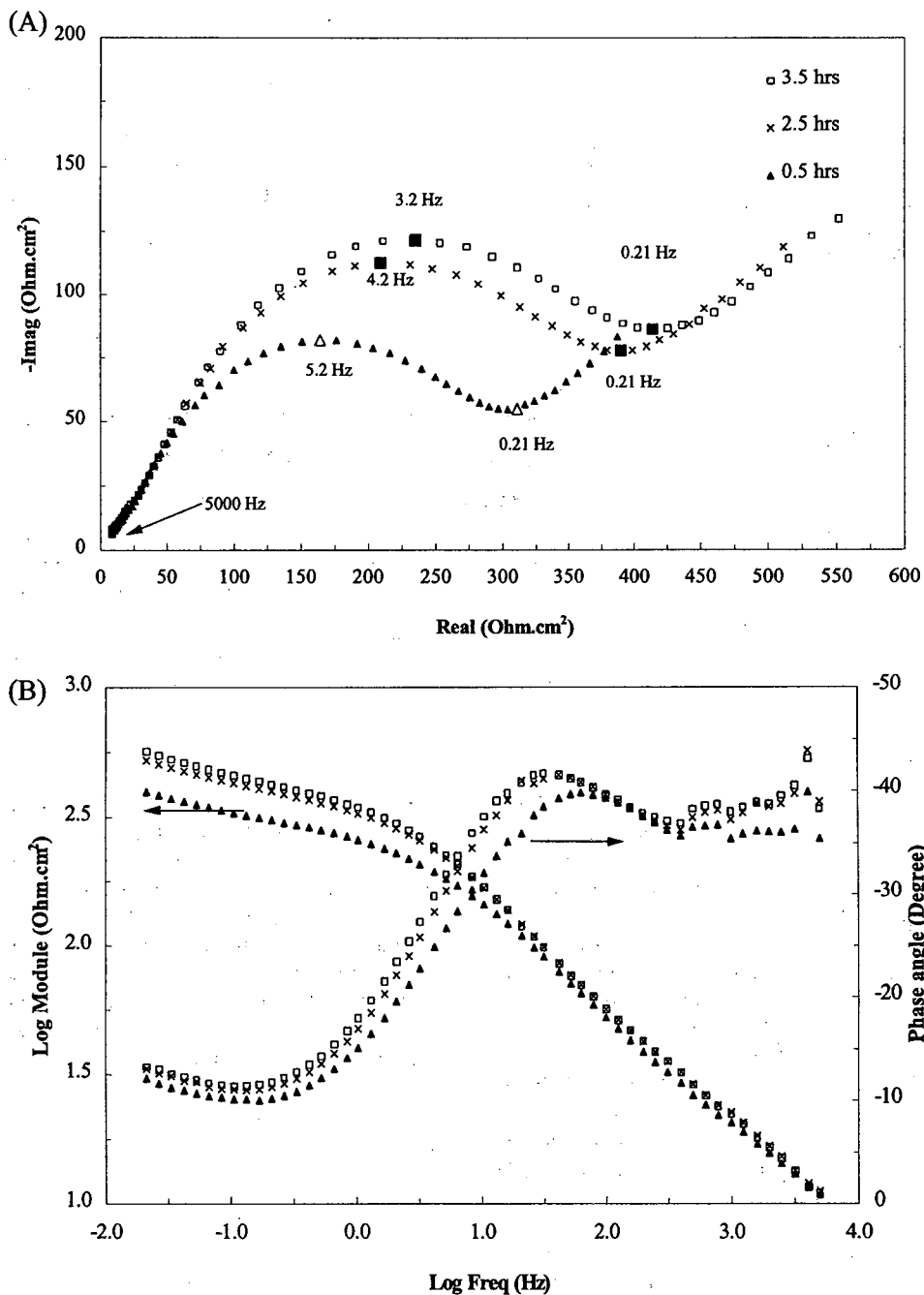


Fig. 11. EIS spectra for Froude number 9 slug flow at different exposure times in 100% ASTM saltwater flow loop system with 100 ppm inhibitor. (a) Nyquist plots (b) Bode plots.

obtained by fitting the EIS spectra using circuit (B) in Fig. 9. For the case with the single loop, EIS data was analyzed by circuit (A). The charge transfer resistance increases with immersion time for all flow conditions except slug flow at Froude number 9. Slug flow at Froude number 9 has the lowest charge transfer resist-

ance, while full pipe flow at liquid velocity of 0.5 m/s has the highest charge transfer resistance. Slug flow with higher Froude numbers (such as 6 and 9) has lower charge transfer resistance than full pipe flow. This indicates that the high rate of turbulence and bubble impact can increase the corrosion rate.

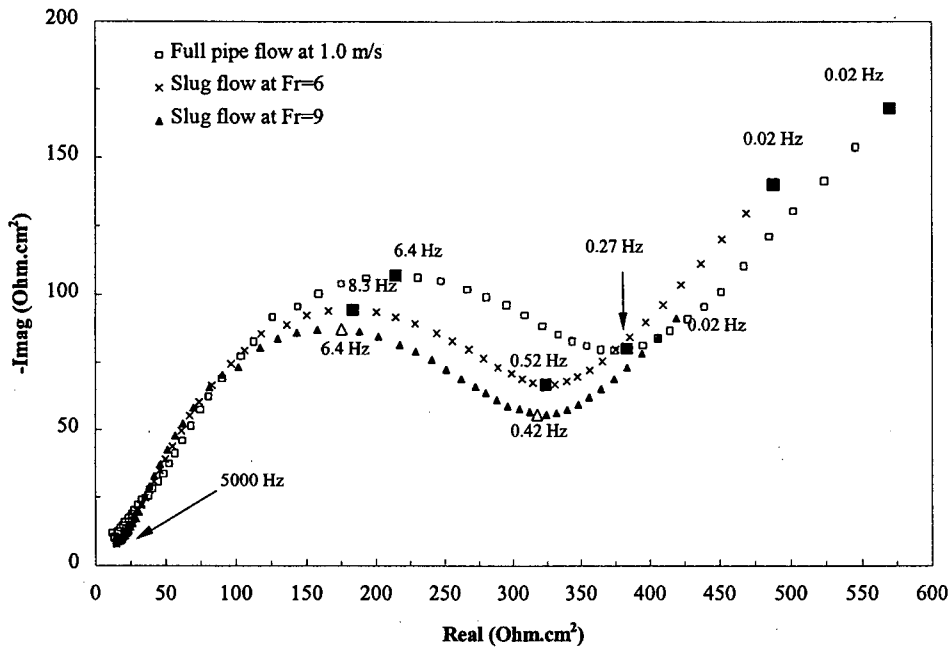


Fig. 12. Nyquist plots of EIS spectra for different flow conditions in 100% ASTM saltwater flow loop system with 25 ppm inhibitor.

### 3.2. Inhibitor tests

A corrosion inhibitor was then added to the system. Fig. 11 presents EIS spectra in 100% ASTM saltwater containing 100 ppm inhibitor for Froude number 9 slug flow at different exposure times. The shape of Nyquist plot for each EIS spectrum seems to have another semicircle at high frequency, which may represent the formation of an inhibitor film. This is in addition to a semicircle for charge transfer process and a diffusion tail at low frequency region. The semicircle of charge transfer process is severely depressed and the

slope of diffusion tail is less than 45°. These could result from the porous inhibitor film formed on the metal surface. The diffusion impedance element suggests that the electrochemical processes might be controlled by the active species diffusing away from the metal surface or corrosion products diffusing away from the metal surface through the inhibitor film. The charge transfer resistance increases with time. The data at very high frequency are unable to be detected because of the limitation of the instrument. A maximum frequency of only 5000 Hz is attainable. However, in the Bode phase plots, a slight dip in the two merging phase angle maximum around 400 Hz is still seen. This could suggest that the electrochemical process occurring at high frequency is the formation of an inhibitor film. In the Bode impedance plots, the module at low frequency region increases with time, which indicates that the corrosion rate decreases with immersion time.

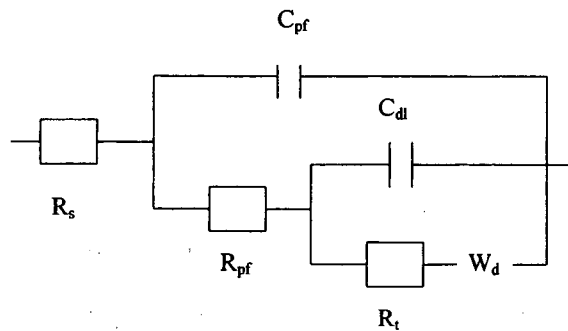


Fig. 13. Equivalent circuit model for fitting EIS data in 100% ASTM saltwater flow loop system with inhibitor.  $R_{pf}$  and  $C_{pf}$ , inhibitor film resistance and capacitance;  $W_d$ , diffusion impedance.

A comparison of EIS Nyquist plots for 100% ASTM saltwater with 25 ppm inhibitor under different flow conditions is shown in Fig. 12. The shape of Nyquist plot appears similar to Fig. 11. The charge transfer resistance decreases with an increase in turbulence. The circuit, as shown in Fig. 13, was used to describe the electrochemical processes in the presence of inhibitor for 100% water cut for each flow condition. Here,  $C_f$  is the inhibitor film capacitance, which is also a constant phase element and  $R_{pf}$  is the pore resistance arising by the formation of conducting paths

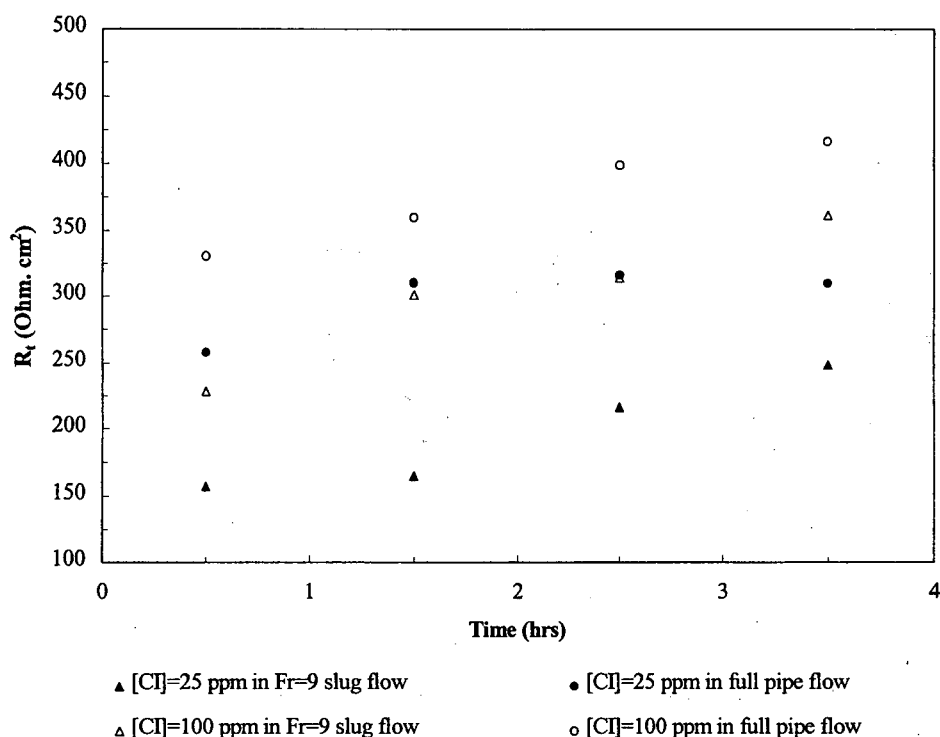


Fig. 14. Charge transfer resistance vs time for different flow conditions in 100% ASTM saltwater flow loop system with different concentrations of inhibitor.

in the inhibitor film [12]. The nested circuits are used to indicate that pores in the film can cause corrosion by providing areas where the electrolyte has direct access to the metal surface. When there are pores within the inhibitor film, the active species of electrolyte can pass through the pores to approach the metal surface. The electrochemical processes with inhibitor include both kinetic and diffusion processes. The diffusion process is described by the Warburg impedance,  $W_d$ . The other elements are the same as the circuit (A) in Fig. 9.

The charge transfer resistance,  $R_t$ , obtained by the circuit as shown in Fig. 13 and corresponding to 25 and 100 ppm inhibitor is presented in Fig. 14. The  $R_t$  for slug flow is lower than full pipe flow at both inhibitor concentrations. This results from the much higher turbulence and bubble impact in the mixing zone of slug. These flow characteristics reduce the inhibition performance of corrosion inhibitor and hence do not decrease the corrosion rate effectively.

### 3.3. Effects of the addition of oil on inhibitor performance

When oil is added to the system, significant changes are noted. Fig. 15 shows the EIS spectra in 80% water

cut with 100 ppm inhibitor under Froude number 9 slug flow at different exposure times. In the presence of oil, the Nyquist plots show that the loop at the high frequency seems to appear after immersion of 2.5 h, which can be seen in Bode phase plot. It suggests the formation of an inhibitor film. When compared to Fig. 11, the charge transfer resistance is much larger, which indicates a lower corrosion rate. The above is expected since the inhibitor used was oil soluble and more inhibitor would be transported to the surface when oil was present in the fully mixed flow.

## 4. Conclusions

The EIS technique can be used to study the corrosion and inhibition processes in multiphase flow conditions, such as full pipe and slug flow.

For full pipe flow at the higher liquid velocities, a second loop appears in the low frequency region, which could be caused by formation of a porous corrosion product layer. The second loop at low frequencies is found in slug flow at Froude number of 4 and 6, however, it is not present in slug flow at Froude number 9. This results from the removal of the product layer at the high rate of shear stress and localized

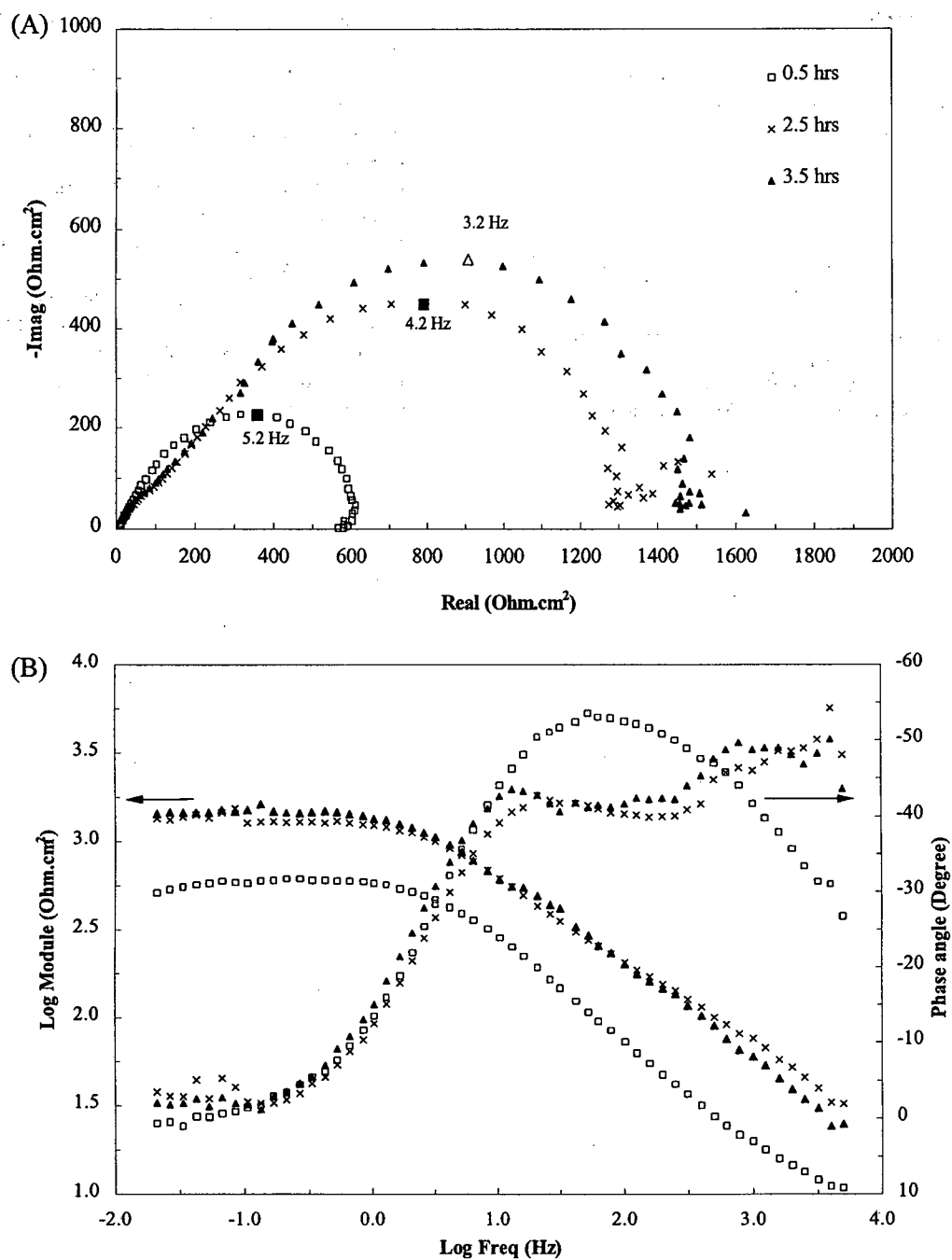


Fig. 15. EIS spectra for Froude number 9 slug flow at different exposure times in 80% water cut flow loop system with 100 ppm inhibitor.

turbulence in the mixing zone of slug at the high Froude number.

The corrosion process in the presence of inhibitor in 100% water cut seems to include charge transfer and diffusion processes. Slug flow reduces the inhibition

performance due to the high shear stress and localized turbulence. In the presence of oil, the inhibition performance of this inhibitor is increased. The diffusion process is not the rate controlling step under effects of oil.

### Acknowledgements

The authors acknowledge assistance by Dr. T. Hong and Dr. M. Gopal at Corrosion in Multiphase Systems Center at Ohio University.

### References

- [1] Jyi-Yu Sun, W.P. Jepson, 1992, SPE Paper 24787, 215.
- [2] H.J. Choi, R.L. Cepulis, 1987, in: SPE Production Engineering, p. 325.
- [3] W.P. Jepson, 1987, 3rd Int. Conf. on Multiphase Flow, The Hague, Netherlands, 187.
- [4] W.P. Jepson, M. Gopal, 1995, 7th Int. Conf. on Multiphase Flow, Wilson, A., MEP, London, 51.
- [5] A.S. Green, B.V. Johnson, H.J. Choi, 1990, SPE Paper 20685, 677.
- [6] X. Zhou, W.P. Jepson, 1994, NACE CORROSION/94, Paper No. 94026.
- [7] M. Gopal, A. Kaul, 1995, NACE CORROSION/95, Paper No.105.
- [8] H. Chen, 1994, NACECORROSION/94, Paper No. 32.
- [9] A. Edwards, et al., Corrosion Science 36 (2) (1994) 135.
- [10] L. Jiang, M. Gopal, Journal of Energy Resources Technology 120 (1998) 67.
- [11] F. Mansfeld, H. Shih et al., 1993, Electrochemical Impedance: Analysis and Interpretation, J.R. Scully, ASTM STP 1188, ASTM, Philadelphia, 37.
- [12] F. Mansfeld, M. Kendig, S. Tsai, Corrosion Science 23 (4) (1983) 317.